Cancer Cell International

https://doi.org/10.1186/s12935-026-04187-5

Article in Press

Divergent effects of topical deferoxamine treatment on skin and cancer cells uncovers its potential as a safe radioprotective agent in oncological applications

Received: 18 July 2025

Accepted: 13 January 2026

Published online: 11 February 2026

Cite this article as: Ledwon J.K., Progri B., Hallman T. *et al.* Divergent effects of topical deferoxamine treatment on skin and cancer cells uncovers its potential as a safe radioprotective agent in oncological applications. *Cancer Cell Int* (2026). https://doi.org/10.1186/s12935-026-04187-5

Joanna K. Ledwon, Bianka Progri, Taylor Hallman, Kathryn R. Reisner, Ariel E. Figueroa, Anitesh Bajaj, Parul Rai, Gabrielle C. Rodriguez, Sofia Aronson & Arun K. Gosain

We are providing an unedited version of this manuscript to give early access to its findings. Before final publication, the manuscript will undergo further editing. Please note there may be errors present which affect the content, and all legal disclaimers apply.

If this paper is publishing under a Transparent Peer Review model then Peer Review reports will publish with the final article.

ARTICLE IN PRESS

© The Author(s) 2026. **Open Access** This article is licensed under a Creative Commons Attribution-NonCommercial-NoDerivatives 4.0 International License, which permits any non-commercial use, sharing, distribution and reproduction in any medium or format, as long as you give appropriate credit to the original author(s) and the source, provide a link to the Creative Commons licence, and indicate if you modified the licensed material. You do not have permission under this licence to share adapted material derived from this article or parts of it. The images or other third party material in this article are included in the article's Creative Commons licence, unless indicated otherwise in a credit line to the material. If material is not included in the article's Creative Commons licence and your intended use is not permitted by statutory regulation or exceeds the permitted use, you will need to obtain permission directly from the copyright holder. To view a copy of this licence, visit http://creativecommons.org/licenses/by-nc-nd/4.0/.

ARTICLE IN PRESS

Divergent effects of topical deferoxamine treatment on skin and cancer cells uncovers its potential as a safe radioprotective agent in oncological applications

Joanna K. Ledwon,[1,2*] Bianka Progri,[2] Taylor Hallman,[2] Kathryn R. Reisner,[2] Ariel E. Figueroa,[1,2] Anitesh Bajaj,[1] Parul Rai,[2] Gabrielle C. Rodriguez,[2] Sofia Aronson,[1] Arun K. Gosain[1,2*]

[1] Northwestern University Feinberg School of Medicine, Division of Plastic Surgery, Chicago, Illinois, United States of America

[2] Ann and Robert H. Lurie Children's Hospital of Chicago, Department of Plastic and Reconstructive Surgery, Stanley Manne Children's Research Institute, Chicago, Illinois, United States of America

ARTICLE IN PRESS

* Corresponding authors

E-mail: jledwon@luriechildrens.org

E-mail: argosain@luriechildrens.org

Abstract

Background: Deferoxamine Intradermal Delivery Patch (DIDP; TauTona Group) represents a novel experimental therapeutic modality with the potential to mitigate radiation-induced skin injury in breast cancer patients undergoing radiotherapy. Nonetheless, the safety profile

ARTICLE IN PRESS

of DIDP in oncological applications has not been extensively explored. Thus, this study aims to investigate the effect of DIDP on mammary tumor cell biology using a murine xenograft human breast cancer model.

Methods: A xenograft human breast cancer model was established by engrafting human-derived MCF7-Luc2 breast cancer cells into the mammary fat pads of female NCG mice. Tumor growth was monitored weekly using the Lago X Bioluminescence Imaging System. The size and volume of excised tumors were recorded. The effect of DIDP treatment on skin and tumor tissue were evaluated using qRT-PCR, immunofluorescence staining, and TUNEL staining.

Results: Our findings demonstrate that topical deferoxamine treatment does not significantly affect tumor growth and cancer cell proliferation in a xenograft human breast cancer model, indicating its safety in oncological settings. Interestingly, mice treated with DIDP exhibited a significant increase in cancer cell apoptosis, suggesting a potential regulatory effect of DIDP on this pathway in cancer cells residing in deeper tissue.

Conclusions: These results support the use of DIDP as a safe radioprotective agent that does not enhance tumor progression. Further studies are warranted to explore the mechanistic role of DIDP in regulating cancer cell apoptosis and its broader implications for cancer therapy.

Keywords: radiation induced injury, breast cancer, deferoxamine, radioprotective therapy

Introduction

Each year, over 2 million women worldwide are diagnosed with breast cancer, which remains the leading cause of cancer-related death among women [1, 2]. Radiation therapy is one of the most common and effective treatments for these patients, playing a crucial role in improving outcomes and reducing recurrence rates [3, 4]. Despite drastic improvements in

ARTICLE IN PRESS

radiation technology and treatment protocols, radiation toxicity in the normal surrounding tissue caused by radiation therapy remains a concerning health problem [5]. Thus, the incorporation of radioprotective modalities into cancer treatment protocols is necessary.

Recent studies have provided strong evidence on the radioprotective effect of deferoxamine (DFO), a free-radical scavenger and iron chelator [6-11]. DFO has been shown to reduce reactive oxygen species, stabilize hypoxia-inducible factor 1-alpha (HIF-1) [12], and mediate neovascularization through vascular endothelial growth factor (VEGF) signaling [13]. These cellular events yield several downstream benefits, including enhanced wound healing [14, 15], improved vascularization [9], and radioprotection of the skin [6, 11, 16, 17]. Radiated skin treated with DFO has shown increased dermal thickness and vascularity, reduced stiffness and fibrosis, and greater elasticity [6, 8, 16, 17].

Previous studies have suggested both pro- [18, 19] and anti-neoplastic [20-24] activity of DFO and its derivatives in various malignancies, including different types of breast cancer. However, these studies have been largely conducted *in vitro*, with direct application of DFO to tumor cells, rather than using a topical drug formulation or systemic drug administration *in vivo*. It is crucial to investigate whether the topical application of DFO exhibits any pro-neoplastic activity *in vivo* to determine its safety for direct translational application, particularly for the novel indication of preventing radiation-induced skin injury in oncological settings.

Topical administration of DFO via Intradermal Delivery Patch (DIDP; TauTona Group) is a novel and convenient method for delivering DFO without compromising its ability to mitigate radiation-induced skin injury [12, 14, 15]. Demonstrating the oncologic safety of DIDP is a prerequisite for its translational application. Yet, its use in the context of malignancy has not been studied *in vivo*. Thus, this study investigates the impact of DIDP on

ARTICLE IN PRESS

tumor growth, cancer cell proliferation, and vascularization in a xenograft human breast cancer model to verify its safety in oncological applications.

Materials and methods

Animal model and study design

A xenograft human breast cancer model was established using 8- to 10-week old immunodeficient female albino mice (NCG; Charles River Laboratories) and a human-derived breast cancer cell line expressing the luciferase reporter gene (MCF7-Luc2; ATCC), following the protocol developed by others (Fig. 1A) [25]. The MCF7-Luc2, a light-producing cell line, allows detection and semi-quantitative analysis of tumor growth *in vivo* [26-28]. In order to facilitate the growth of estrogen receptor-positive tumors, 60-day slow-release 17β-estradiol reservoir implant (Belmatech) was implanted into the dorsal flank of experimental mice according to previously described methods [29-32]. Implant insertion was performed 3-5 days in advance of planned xenografting to ensures that circulating estrogen levels are adequate to support tumor growth [31]. On the day of cancer cell injection, a small incision between the fourth nipple and the midline was made to enable orthotopic cancer cell injection. Next, 1 million MCF7-Luc2 breast cancer cells in 120 l of Phosphate Buffered Saline (PBS) were engrafted into the mammary fat pad using a syringe. The incision was closed with sutures. All surgical procedures were performed under a sterile hood. *In vivo* tumor growth was monitored weekly using the LAGO bioluminescence imaging system (Spectral Instruments Imaging) following luciferin injection. Luciferin (150 mg/kg) was administered intraperitoneally to detect luciferase activity in MCF7-Luc2 breast cancer cells, and the emitted light was captured through a bioluminescence assay. The Aura software (Spectral Instruments Imaging) was utilized to visualize and measure tumor growth. Once the tumor reached bioluminescence intensity ~$1x10^8$ photons/second (approximately 2 weeks

ARTICLE IN PRESS

after cancer cell injection), mice were randomly divided into the control and experimental groups (n 10 per group). The experimental group received 1.5 cm x 2 cm DFO patches, consisting of 1 mg/cm^2 of DFO, applied daily for 30 days, and the control group received a placebo dressing (veterinary elastic adhesive tape only) over the surgical site to ensure that the tumor cells in both groups had the same conditions to grow. Detailed information about the DFO patch formulation was provided previously by others [12]. The patch was secured with a veterinary elastic adhesive tape wrapped around the mice belly to keep it in place at all times. After 30 days of treatment with either DFO or the placebo dressing, the tumor was excised, and mass weight, length and width measurements were recorded. Samples of the skin overlying the tumor (treated with DIDP or placebo) and the tumor tissue were harvested and carefully divided into two comparable halves. To minimize regional bias, the tumor tissue was cut along the longest axis to ensure that each half contained representative areas of the tumor tissue. One half was preserved in 10% formalin and embedded in paraffin for immunofluorescence (IF) staining, and the other half was preserved in All Protect Reagent for RNA extraction. This approach was applied consistently across all samples.

ARTICLE IN PRESS

Cell culture

MCF7-Luc2, a human breast cancer cell line expressing luciferase, was purchased from ATCC (USA). The cells were cultured in 5% CO_2 at 37°C in ATCC-formulated Eagle's Minimum Essential Medium (EMEM; ATCC) supplemented with 10% fetal bovine serum (FBS, Gibco), 0.01 mg/ml human recombinant insulin (Lonza), and 4 µg/ml blasticidin (Thermo Scientific Chemicals). The cells were grown to 70-80% confluency and harvested on the day of cancer cell injection. Each mouse received an injection of 1 million cells resuspended in 120 µl of PBS.

Bioluminescence assay

ARTICLE IN PRESS

Tumor growth was monitored using the Lago X Bioluminescence Imaging System (Spectral Instruments Imaging), which detects light emission from luciferase-expressing cells upon interaction with the luciferin substrate. The bioluminescence signal is highly sensitive and quantitative, providing precise and reproducible measurements of tumor progression over time. Briefly, mice were anesthetized with isoflurane inhalation. IVISbrite D-Luciferin potassium salt (150 mg/kg; Revvity) was administered intraperitoneally, and imaging was initiated 10 minutes post-injection. Images were captured using the system's preset Easy Mode settings. Quantitative analysis of the bioluminescence signal, expressed as total emission (photons/second), was performed using Aura Imaging software (Spectral Instruments Imaging). The signal was measured specifically in the tumor region by defining a region of interest, which was consistently applied across different images.

Tumor volume and weight measurements

Considering the small tumor size and its location in deeper tissue as a result of orthotopic cancer cell injection, *in vivo* tumor volume measurements using caliper are not accurate and prone to investigator error. Therefore, we report caliper measurements only at the study endpoint. On the day of tissue harvesting, the tumor was excised, and its volume and weight were recorded. Caliper measurements of the greatest tumor length and width were used to calculate tumor volume. Tumor volume was calculated using the following formula: volume = (length x width^2)/2. The correlation between bioluminescence signal and tumor volume at the study endpoint was evaluated using Spearman test. A non-parametric test was selected because the data did not pass the normality test.

Total RNA extraction

The collected skin and tumor samples, preserved in AllProtect Reagent (Qiagen), were homogenized using a TissueLyser LT homogenizer (Qiagen) equipped with 7 mm stainless

ARTICLE IN PRESS

steel beads (Qiagen) for three cycles of 10 minutes each at 50,000 Hz in a cold room. Total RNA was extracted using RNAeasy Mini Kit (Qiagen) with DNase I treatment (Qiagen) according to the manufacturer's protocol. The tissue homogenization and extraction procedures above have been previously described in detail [33].

Quantitative real-time PCR analysis (qRT-PCR)

The qRT-PCR analysis was performed on QuantStudio 6 Flex Real-Time PCR Systems (Applied Biosystems) using TaqMan Assay (Applied Biosystems) [34]. The commercially available TaqMan probes for vascular endothelial growth factor A (Mm00437306_m1 and Hs00900055_m1) and pyruvate dehydrogenase kinase 1 (Mm00554300_m1 and Hs01561847) genes were mixed with TaqMan Fast Advanced Master Mix according to the protocol described previously [34]. The gene expression was calculated using the threshold cycle and the $2^{-\Delta\Delta CT}$ methods [35]. The expression of the gene of interest was normalized to 18S ribosomal RNA (Mm03928990) and TATA-box binding protein (Hs00427620) reference genes for skin and tumor samples, respectively.

Immunofluorescence staining

Immunofluorescence **(**IF) staining was performed on 4 m cross-sections preserved in 10% formalin and embedded in paraffin, following the protocol described previously [33, 36]. Tissue sections were incubated with the following primary antibodies: anti-Ki-67 (1:500; Invitrogen, 14-5698-82), anti-CD31 (1:100; Abcam ab28364), and anti-HIF-1 (1:200; Invitrogen PA1-16601) at 4C overnight. The following fluorochrome-conjugated secondary antibodies were incubated at room temperature for 1 hour: donkey anti-rabbit IgG Alexa Fluor 546 (1:200; Invitrogen, A10040) and goat anti-rat IgG Alexa Fluor 647 (1:200; Invitrogen, A-21247). Nuclei were stained with 1 μg/ml DAPI (Invitrogen). To assess staining specificity, control staining was performed without primary antibodies. Stained

ARTICLE IN PRESS

slides were photographed on a Zeiss LSM 880 laser scanning confocal microscope using 40x water immersion objective or Keyence microscope using 10x, 25x and 40x objectives. Imaging conditions were optimized for each target protein using control tissue and then applied to the corresponding experimental samples. Total fluorescence intensity, percentage area of the positive fluorescence signal, and the ratio of positive cells were assessed using ImageJ software (National Institutes of Health).

Hypoxia-inducible factor 1-alpha (HIF-1) fluorescence intensity quantification

Hypoxia-inducible factor 1-alpha (HIF-1) protein abundance was assessed in skin tissue by measuring the total fluorescence intensity (sum of pixel intensities) normalized to the total number of cells using ImageJ. The results are presented as the relative changes of total fluorescence signal intensity per cell between control and DFO-treated samples. The mean value for control was set as 1. The analysis was performed on at least four randomly selected microscopic fields for each analyzed specimen. At least nine specimens (n 9) were analyzed in both the control and experimental groups.

ARTICLE IN PRESS

Blood vessel density quantification

Blood vessel density was quantified in CD31-immunofluorescent-stained skin tissue using ImageJ. Data are presented as the relative changes of the percentage area positive for CD31. The mean value for control was set as 1. The analysis was performed on at least four randomly selected microscopic fields for each analyzed specimen. At least 10 specimens (n 10) were analyzed in both the control and experimental groups.

Cell proliferation quantification

ARTICLE IN PRESS

Cell proliferation was assessed in Ki-67-immunofluorescent-stained tumor tissue using ImageJ and calculated as the number of Ki-67 positive cells divided by the total number of cells detected based on DAPI staining. The analysis was performed on at least four randomly selected microscopic fields for each analyzed specimen. At least nine specimens (n 9) were analyzed in both the control and experimental groups. Data are presented as the percentage of Ki-67 positive cells.

TUNEL staining

TUNEL staining was performed using the TUNEL Assay Kit – BrdU-Red (Abcam). The manufacturer's protocol was modified by incubating the slides with 40 μg/ml Proteinase K solution (Qiagen) instead of the 20 μg/ml, to improve the DNA Labeling Solution penetration. Stained slides were photographed on a Zeiss LSM 880 laser scanning confocal microscope using 25x oil immersion objective. Data are presented as the fold change of the number of apoptotic cells divided by the total number of cells detected based on DAPI staining. The mean value for control was set as 1. The analysis was performed on at least five randomly selected microscopic fields for each analyzed specimen. At least seven specimens (n 7) were analyzed in both the control and experimental groups.

ARTICLE IN PRESS

Statistical analysis

The statistical significance of the results was assessed using the Mann-Whitney test in GraphPad Prism v.9.2.0 software (GraphPad Software, Inc.). *p*-value < 0.05 was considered significant. Error bars represent standard deviation (SD) or standard error of the mean (SEM).

Results

DIDP exhibits pro-vasculogenic effect on skin

ARTICLE IN PRESS

IF staining revealed a significant 2.42-fold increase in hypoxia-inducible factor 1-alpha (HIF-1) abundance in mouse skin after a 30-day treatment with DFO patches compared to the control group ($p < 0.0001$; Fig. 1B,C). Accompanying HIF-1 stabilization, we observed a significant increase in the expression of vascular endothelial growth factor A (*Vegfa*; $p = 0.0056$), but not in pyruvate dehydrogenase kinase 1 (*Pdk1*; $p = 0.1164$), both downstream targets of HIF-1, in the skin of DFO-treated mice, as shown by qRT-PCR (Fig. 1D). Furthermore, skin sections stained for platelet endothelial cell adhesion molecule (CD31), a specific marker of endothelial cells, demonstrated an increase in blood vessel density in DFO-treated mice by an average of 43% ($p < 0.0001$) compared to control mice (Fig. 1E-F). These results confirm successful administration of DFO via DIDP and positive effect of topical DFO on skin vascularization via the HIF-1-dependent pathway.

Topical DFO applied via DIDP does not penetrate deeper tissue

Due to the heterogeneous expression of HIF-1 in tumor cells and using only half of the tumor for IF staining, direct analysis of HIF-1 stabilization on IF-stained slides was not possible. Therefore, to investigate the ability of DIDP-delivered DFO to penetrate deeper tissues, we assessed the expression of HIF-1 target genes in tumor samples. qRT-PCR analysis revealed no significant changes in *VEGFA* and *PDK1* expression in tumors extracted from mice treated with DIDP compared to the control group (Fig. 2A). These data indicate that DFO applied via DIDP has a limited ability to penetrate deeper tissue and likely does not affect tumor vascularization.

Topical DFO applied via DIDP does not stimulate tumor growth located in deeper tissue

ARTICLE IN PRESS

To investigate a direct effect of DIDP treatment on tumor development, we measured size of the tumor every 7 days over a 30-day period using a bioluminescence assay following luciferin injection (Fig. 2B). This technique relies on the expression of luciferase within tumor cells, allowing for non-invasive, real-time monitoring of tumor growth *in vivo* [37]. Throughout the experiment, no statistically significant differences in tumor size were detected between groups. However, a trend toward reduced tumor size was observed in the DIDP-treated group from day 21 (Fig. 2B,C). These findings suggest that DIDP treatment does not promote tumor growth and may exert a mild inhibitory effect on tumor progression. Additionally, tumor weight and volume measured after tumor excision at the study endpoint were also not significantly different between groups (Fig. 2D,E), further supporting our previous findings. The correlation analysis between the excised-tumor volume data and the last bioluminescence data demonstrated a strong positive correlation ($r = 0.759$; $p = 0.0003$).

Topical DFO applied via DIDP may indirectly inhibit cancer cell survival

To further investigate the effect of DIDP on cancer cell biology, additional analyses were conducted to assess tumor cell proliferation and apoptosis. While the DIDP-treated group showed a slight decrease in the number of Ki-67 positive cells compared to control (FC = 0.876, $p = 0.4363$), the difference was not statistically significant (Fig. 3A,B). Similarly, although the average *CCND1* expression was lower in the DFO-treated group, the observed difference was not statistically significant (Fig. 3C). Although not statistically significant, the observed reductions in both Ki-67 positive cells and *CCND1* expression are consistent with a potential mild anti-proliferative effect.

To assess the effect of the treatment on cancer cell viability, we performed TUNEL staining that detects DNA fragmentation associated with apoptotic cell death. Compared to the control

ARTICLE IN PRESS

group, a significant 1.58-fold increase in the percentage of Brdu-red-positive cells was observed in the tumor tissue collected from DIDP-treated mice (p = 0.0115; Fig. 3D,E), indicating an enhanced level of apoptosis. These findings suggest that DIDP applied onto skin promotes cancer cell death in deeper tissue, as evidenced by increased DNA fragmentation detected through TUNEL assay, which may result from iron depletion in the tumor microenvironment. Altogether, these findings provide preliminary evidence that DIDP may indirectly influence tumor cell behavior located in deeper tissues, leading to cancer growth inhibition and warranting further in-depth studies to clarify its long-term biological effects.

DISCUSSION

Radiation-induced skin injury is a key challenge in the care of cancer patients undergoing radiation therapy [5]. While radiation therapy is crucial for cancer treatment, it can profoundly compromise skin tissue, resulting in complications such as erythema, desquamation, and ulceration [38-40]. These early and late effects are mediated by progressive epidermal and endothelial injury, inflammation, and subsequent pro-fibrotic response [41]. DIDP is one of the most promising novel radioprotective treatments shown to effectively mitigate radiation-induced fibrosis in a murine model [16, 42]. However, its use in oncology requires thorough evaluation to ensure that DIDP application does not promote tumor progression. To assess this potential risk, we investigated DIDP in a murine xenograft model of human breast cancer. The present study examined how cellular iron deficiency in surrounding tissue affects cancer cell signaling pathways that are key to cell proliferation, apoptosis, and tumor angiogenesis. We provide evidence that cellular iron deficiency through DIDP topical application contributes to HIF-1 stabilization and angiogenesis in skin without magnifying the tumorigenic potential of underlying tumor cells.

ARTICLE IN PRESS

DIDP offers a convenient way to apply DFO on the area exposed to radiation therapy to protect healthy skin tissue. In contrast to drug injection or systemic application, DIDP allows for local topical administration, limiting unwanted systemic effects. We demonstrated that HIF-1 stabilization and improved vascularization in response to DIDP treatment were restricted to skin tissue that was in direct contact with the drug. Consistent with these findings, others have shown that DFO administered via patch successfully infiltrates the skin barrier and its concentration declines with skin depth [12]. The pro-angiogenic effect of DFO noted in this study parallels the findings reported by other group showing improved vascularity in irradiated skin treated with topical DFO [8]. Thus, our study strongly suggests that DIDP does not penetrate deeper tissue, limiting its radioprotective effect to treated skin.

We also observed no significant differences in the tumorigenic potential of cancer cells between the control and DIDP-treated groups, as demonstrated by the bioluminescence assay used to monitor tumor growth, as well as measurements of tumor weight and volume. These findings were further supported by IF staining of Ki-67, which showed a trend toward reduced cancer cell proliferation in the DIDP-treated group, although the difference was not statistically significant. This result aligns with previous studies showing that cell viability and proliferation are reduced in cells treated with iron chelators [43-47], while the addition of transferrin stimulates breast cancer cell proliferation *in vitro* [45]. Substantial evidence indicates that iron plays a significant role in cancer development and progression, [48-58] and numerous studies have shown that iron chelators, including DFO, possess strong anti-tumor activity [20, 43, 44, 50, 54, 56, 59-61]. Consistent with these findings, we observed that, despite the lack of direct contact between DIDP and cancer cells, DIDP treatment promotes apoptosis in these cells. Our findings align with previous research showing increased cancer cell apoptosis due to iron depletion resulting from the injection of iron chelators or a low-iron diet [47, 50, 62, 63]. Interestingly, this effect contrasts with the previous observations in the

ARTICLE IN PRESS

skin tissue directly exposed to DIDP [12]. Given previous research demonstrating that DFO reduces iron uptake and promotes iron efflux *in vitro* [43], we speculate that the observed increase in the number of apoptotic cells in tumors extracted from DIDP-treated mice may result from iron depletion in the tumor microenvironment following DIDP treatment. Altogether, decreased cell proliferation and increased cell apoptosis in tumors can lead to reduced cancer cell survival, potentially hindering tumor growth and metastasis. Therefore, our results suggest that topical iron chelation via DIDP application may impair tumor progression by indirectly disrupting essential pathways involved in tumor growth and survival.

The divergent effects of topical deferoxamine treatment on skin and cancer cells can be associated with an increased demand for iron by cancer cells, making them vulnerable to iron deprivation. Iron chelators can disrupt cancer cell growth and metabolism by reducing iron availability, potentially leading to cell death [64, 65], and iron chelators have been extensively studied for their potential to inhibit cancer cell growth and tumor progression [47, 66, 67].

Importantly, while 30-day treatment is sufficient to detect the pro-angiogenic effect of DIDP in treated skin, this time period may not be long enough to fully elucidate DIDP effects on tumorigenesis, including cancer cell metastasis. There are also many differences between various types of cancer and their ability to metastasize. Thus, further testing on different cell types with extended observation time is needed. Despite these limitations, this study presents significant data identifying DIDP as a safe radioprotective agent in oncological applications.

Conclusions

This study reinforces the importance of verifying the oncological safety of radioprotective interventions in controlled *in vivo* conditions. Our findings suggest that the ability of DFO to exert regenerative and pro-vasculogenic effects when applied topically is limited to

ARTICLE IN PRESS

superficial tissues. Thus, topical DFO treatment most likely presents minimal risk of potentially accelerating the growth of residual cancer cells in deeper tissues, as indicated by no significant difference in tumor growth, cancer cell proliferation, and vascularization in DIDP-treated mice compared to control. Moreover, topical DFO treatment may indirectly promote cancer cell apoptosis by depleting iron in the underlying skin.

List of Abbreviations

DIDP - Deferoxamine Intradermal Delivery Patch

DFO - Deferoxamine

HIF-1 - Hypoxia-inducible factor 1-alpha

VEGFA - Vascular endothelial growth factor A

PBS - Phosphate Buffered Saline

IF staining – Immunofluorescence staining

EMEM - Eagle's Minimum Essential Medium

FBS - Fetal bovine serum

qRT-PCR - Quantitative real-time PCR

PDK1- Pyruvate dehydrogenase kinase 1

CD31 - Platelet endothelial cell adhesion molecule

ARTICLE IN PRESS

Author Contributions

Joanna K. Ledwon: Conceptualization (lead); Funding acquisition (equal); Data curation (equal); Formal analysis (equal); Investigation (equal); Methodology (lead); Visualization (lead); Supervision (equal); Writing – original draft (lead). **Bianka Progri:** Data curation (equal); Formal analysis (equal); Investigation (equal). **Taylor Hallman:** Investigation (supporting). **Kathryn R. Reisner:** Investigation (supporting). **Ariel E. Figueroa:** Investigation (supporting). **Anitesh Bajaj:** Investigation (supporting). **Parul Rai:** Investigation (supporting). **Gabrielle C. Rodriguez:** Investigation (supporting). **Sofia**

ARTICLE IN PRESS

Aronson: Conceptualization (supporting); **Arun K. Gosain:** Conceptualization (supporting); Funding acquisition (equal); Supervision (equal); Writing – review and editing (lead).

Data Availability Statement

The data that support the findings of this study are available from the corresponding author upon reasonable request.

Ethics Statement

The animal work was approved by Northwestern University Institutional Animal Care and Use Committee. All procedures were conducted according to the protocol number IS00023166 and in compliance with the Guide for the Care and Use of Laboratory Animals published by National Institute of Health. The animals were housed in animal facility at Center for Comparative Medicine (Northwestern University, Chicago, IL, USA) accredited by the Association for Assessment and Accreditation of Laboratory Animal Care International.

Conflict of Interest

The authors confirm that there are no conflicts of interest.

ARTICLE IN PRESS

Acknowledgements

Histology and Microscopy Services were provided by the Histology and Microscopy Group at Stanley Manne Children's Research Institute, affiliated with Ann & Robert H. Lurie Children's Hospital of Chicago. Animal work was performed at the Center for Comparative Medicine at Northwestern University. Bioluminescence imaging work was performed at the Northwestern University Center for Advanced Microscopy (RRID: SCR_020996) generously supported by NCI CCSG P30 CA060553 awarded to the Robert H Lurie Comprehensive Cancer Center.

Funding Statement

ARTICLE IN PRESS

This work was supported by the Academic Enrichment Fund Grant number IG930136 awarded by the Department of Surgery at Ann & Robert H. Lurie Children's Hospital of Chicago.

References

1. American Cancer Society. Cancer Statistics. Breast Cancer. Available from: https://www.cancer.org/cancer/types/breast-cancer/about/how-common-is-breast-cancer.html.

2. World Health Organization. Breast cancer; 2022. Available from: https://www.who.int/news-room/fact-sheets/detail/breast-cancer.

3. Miller KD, Nogueira L, Mariotto AB, Rowland JH, Yabroff KR, Alfano CM, et al. Cancer treatment and survivorship statistics, 2019. CA Cancer J Clin. 2019;69(5):363-85.

4. de Boniface J, Szulkin R, Johansson ALV. Survival After Breast Conservation vs Mastectomy Adjusted for Comorbidity and Socioeconomic Status: A Swedish National 6-Year Follow-up of 48986 Women. JAMA Surg. 2021;156(7):628-37.

5. Citrin DE, Prasanna PGS, Walker AJ, Freeman ML, Eke I, Barcellos-Hoff MH, et al. Radiation-Induced Fibrosis: Mechanisms and Opportunities to Mitigate. Report of an NCI Workshop, September 19, 2016. Radiat Res. 2017;188(1):1-20.

6. Mericli AF, Das A, Best R, Rodeheaver P, Rodeheaver G, Lin KY. Deferoxamine mitigates radiation-induced tissue injury in a rat irradiated TRAM flap model. Plastic and reconstructive surgery. 2015;135(1):124e-34e.

7. Flacco J, Chung N, Blackshear CP, Irizarry D, Momeni A, Lee GK, et al. Deferoxamine Preconditioning of Irradiated Tissue Improves Perfusion and Fat Graft Retention. Plastic and reconstructive surgery. 2018;141(3):655-65.

8. Dassoulas KR, Mericli AF, Wang JS, Lei SS, Kim T, Cottler PS, et al. Treatment With Topical Deferoxamine Improves Cutaneous Vascularity and Tissue Pliability in an

ARTICLE IN PRESS

Irradiated Animal Model of Tissue Expander-Based Breast Reconstruction. Ann Plast Surg. 2019;82(1):104-9.

9. Donneys A, Weiss DM, Deshpande SS, Ahsan S, Tchanque-Fossuo CN, Sarhaddi D, et al. Localized deferoxamine injection augments vascularity and improves bony union in pathologic fracture healing after radiotherapy. Bone. 2013;52(1):318-25.

10. Snider AE, Lynn JV, Urlaub KM, Donneys A, Polyatskaya Y, Nelson NS, et al. Topical Deferoxamine Alleviates Skin Injury and Normalizes Atomic Force Microscopy Patterns Following Radiation in a Murine Breast Reconstruction Model. Ann Plast Surg. 2018;81(5):604-8.

11. Tevlin R, Longaker MT, Wan DC. Deferoxamine to Minimize Fibrosis During Radiation Therapy. Adv Wound Care (New Rochelle). 2022;11(10):548-59.

12. Duscher D, Neofytou E, Wong VW, Maan ZN, Rennert RC, Inayathullah M, et al. Transdermal deferoxamine prevents pressure-induced diabetic ulcers. Proc Natl Acad Sci U S A. 2015;112(1):94-9.

13. Weng R, Li Q, Li H, Yang M, Sheng L. Mimic hypoxia improves angiogenesis in ischaemic random flaps. J Plast Reconstr Aesthet Surg. 2010;63(12):2152-9.

14. Duscher D, Trotsyuk AA, Maan ZN, Kwon SH, Rodrigues M, Engel K, et al. Optimization of transdermal deferoxamine leads to enhanced efficacy in healing skin wounds. J Control Release. 2019;308:232-9.

15. Rodrigues M, Bonham CA, Minniti CP, Gupta K, Longaker MT, Gurtner GC. Iron Chelation with Transdermal Deferoxamine Accelerates Healing of Murine Sickle Cell Ulcers. Adv Wound Care (New Rochelle). 2018;7(10):323-32.

16. Lintel H, Abbas DB, Lavin CV, Griffin M, Guo JL, Guardino N, et al. Transdermal deferoxamine administration improves excisional wound healing in chronically irradiated murine skin. J Transl Med. 2022;20(1):274.

ARTICLE IN PRESS

ARTICLE IN PRESS

17. Berry CE, Abbas DB, Griffin M, Lintel H, Guo J, Kameni L, et al. Deferoxamine topical cream superior to patch in rescuing radiation-induced fibrosis of unwounded and wounded skin. J Cell Mol Med. 2024;28(8):e18306.

18. Chen C, Wang S, Liu P. Deferoxamine Enhanced Mitochondrial Iron Accumulation and Promoted Cell Migration in Triple-Negative MDA-MB-231 Breast Cancer Cells Via a ROS-Dependent Mechanism. Int J Mol Sci. 2019;20(19).

19. Liu P, He K, Song H, Ma Z, Yin W, Xu LX. Deferoxamine-induced increase in the intracellular iron levels in highly aggressive breast cancer cells leads to increased cell migration by enhancing TNF-alpha-dependent NF-kappaB signaling and TGF-beta signaling. J Inorg Biochem. 2016;160:40-8.

20. Fryknas M, Zhang X, Bremberg U, Senkowski W, Olofsson MH, Brandt P, et al. Iron chelators target both proliferating and quiescent cancer cells. Sci Rep. 2016;6:38343.

21. Tury S, Assayag F, Bonin F, Chateau-Joubert S, Servely JL, Vacher S, et al. The iron chelator deferasirox synergises with chemotherapy to treat triple-negative breast cancers. J Pathol. 2018;246(1):103-14.

22. Komoto K, Nomoto T, El Muttaqien S, Takemoto H, Matsui M, Miura Y, et al. Iron chelation cancer therapy using hydrophilic block copolymers conjugated with deferoxamine. Cancer Sci. 2021;112(1):410-21.

23. Bajbouj K, Shafarin J, Hamad M. High-Dose Deferoxamine Treatment Disrupts Intracellular Iron Homeostasis, Reduces Growth, and Induces Apoptosis in Metastatic and Nonmetastatic Breast Cancer Cell Lines. Technol Cancer Res Treat. 2018;17:1533033818764470.

24. Brown RAM, Richardson KL, Kabir TD, Trinder D, Ganss R, Leedman PJ. Altered Iron Metabolism and Impact in Cancer Biology, Metastasis, and Immunology. Front Oncol. 2020;10:476.

ARTICLE IN PRESS

ARTICLE IN PRESS

25. Kocaturk B, Versteeg HH. Orthotopic injection of breast cancer cells into the mammary fat pad of mice to study tumor growth. J Vis Exp. 2015(96).

26. Shan L, Wang S, Korotcov A, Sridhar R, Wang PC. Bioluminescent animal models of human breast cancer for tumor biomass evaluation and metastasis detection. Ethn Dis. 2008;18(2 Suppl 2):S2-65-9.

27. Jenkins DE, Hornig YS, Oei Y, Dusich J, Purchio T. Bioluminescent human breast cancer cell lines that permit rapid and sensitive in vivo detection of mammary tumors and multiple metastases in immune deficient mice. Breast Cancer Res. 2005;7(4):R444-54.

28. Baklaushev VP, Kilpelainen A, Petkov S, Abakumov MA, Grinenko NF, Yusubalieva GM, et al. Luciferase Expression Allows Bioluminescence Imaging But Imposes Limitations on the Orthotopic Mouse (4T1) Model of Breast Cancer. Sci Rep. 2017;7(1):7715.

29. Dall G, Vieusseux J, Unsworth A, Anderson R, Britt K. Low Dose, Low Cost Estradiol Pellets Can Support MCF-7 Tumour Growth in Nude Mice without Bladder Symptoms. J Cancer. 2015;6(12):1331-6.

30. Laidlaw IJ, Clarke RB, Howell A, Owen AW, Potten CS, Anderson E. The proliferation of normal human breast tissue implanted into athymic nude mice is stimulated by estrogen but not progesterone. Endocrinology. 1995;136(1):164-71.

31. Gerard C, Gallez A, Dubois C, Drion P, Delahaut P, Quertemont E, et al. Accurate Control of 17beta-Estradiol Long-Term Release Increases Reliability and Reproducibility of Preclinical Animal Studies. J Mammary Gland Biol Neoplasia. 2017;22(1):1-11.

32. Chatzistamou I, Kiaris H. Modeling estrogen receptor-positive breast cancers in mice: is it the best we can do? Endocr Relat Cancer. 2016;23(11):C9-C12.

33. Ledwon JK, Applebaum SA, Progri B, Vignesh O, Gutowski KS, Chang AB, et al. Biological Cover Mitigates Disruption of the Dermal Structure in Mechanically Expanded Skin in a Porcine Model. Int J Mol Sci. 2022;23(21).

ARTICLE IN PRESS

ARTICLE IN PRESS

34. Ledwon JK, Kelsey LJ, Vaca EE, Gosain AK. Transcriptomic analysis reveals dynamic molecular changes in skin induced by mechanical forces secondary to tissue expansion. Sci Rep. 2020;10(1):15991.

35. Livak KJ, Schmittgen TD. Analysis of relative gene expression data using real-time quantitative PCR and the 2(-Delta Delta C(T)) Method. Methods. 2001;25(4):402-8.

36. Ledwon JK, Vaca EE, Huang CC, Kelsey LJ, McGrath JL, Topczewski J, et al. Langerhans cells and SFRP2/Wnt/beta-catenin signalling control adaptation of skin epidermis to mechanical stretching. J Cell Mol Med. 2022;26(3):764-75.

37. Spectral Instruments Imaging. Bioluminescence Imaging System. Available from: https://spectralinvivo.com/imaging-systems/.

38. Borrelli MR, Shen AH, Lee GK, Momeni A, Longaker MT, Wan DC. Radiation-Induced Skin Fibrosis: Pathogenesis, Current Treatment Options, and Emerging Therapeutics. Ann Plast Surg. 2019;83(4S Suppl 1):S59-S64.

39. Singh M, Alavi A, Wong R, Akita S. Radiodermatitis: A Review of Our Current Understanding. Am J Clin Dermatol. 2016;17(3):277-92.

40. Mukesh MB, Harris E, Collette S, Coles CE, Bartelink H, Wilkinson J, et al. Normal tissue complication probability (NTCP) parameters for breast fibrosis: pooled results from two randomised trials. Radiother Oncol. 2013;108(2):293-8.

41. Archambeau JO, Pezner R, Wasserman T. Pathophysiology of irradiated skin and breast. Int J Radiat Oncol Biol Phys. 1995;31(5):1171-85.

42. Perrault D, Chen K, Nazerali R, Wan D. Deferoxamine Intradermal Delivery Patch for Treatment of a Radiation Therapy Associated Breast Wound. Ann Case Rep. 2024;9(3).

43. Ford SJ, Obeidy P, Lovejoy DB, Bedford M, Nichols L, Chadwick C, et al. Deferasirox (ICL670A) effectively inhibits oesophageal cancer growth in vitro and in vivo. Br J Pharmacol. 2013;168(6):1316-28.

ARTICLE IN PRESS

44. Whitnall M, Howard J, Ponka P, Richardson DR. A class of iron chelators with a wide spectrum of potent antitumor activity that overcomes resistance to chemotherapeutics. Proc Natl Acad Sci U S A. 2006;103(40):14901-6.

45. Reddel RR, Hedley DW, Sutherland RL. Cell cycle effects of iron depletion on T-47D human breast cancer cells. Exp Cell Res. 1985;161(2):277-84.

46. Kulp KS, Green SL, Vulliet PR. Iron deprivation inhibits cyclin-dependent kinase activity and decreases cyclin D/CDK4 protein levels in asynchronous MDA-MB-453 human breast cancer cells. Exp Cell Res. 1996;229(1):60-8.

47. Lui GY, Obeidy P, Ford SJ, Tselepis C, Sharp DM, Jansson PJ, et al. The iron chelator, deferasirox, as a novel strategy for cancer treatment: oral activity against human lung tumor xenografts and molecular mechanism of action. Mol Pharmacol. 2013;83(1):179-90.

48. Trowbridge IS, Lopez F. Monoclonal antibody to transferrin receptor blocks transferrin binding and inhibits human tumor cell growth in vitro. Proc Natl Acad Sci U S A. 1982;79(4):1175-9.

49. Shanmugam R, Majee P, Shi W, Ozturk MB, Vaiyapuri TS, Idzham K, et al. Iron-(Fe3+)-Dependent Reactivation of Telomerase Drives Colorectal Cancers. Cancer Discov. 2024;14(10):1940-63.

50. Jiang XP, Wang F, Yang DC, Elliott RL, Head JF. Induction of apoptosis by iron depletion in the human breast cancer MCF-7 cell line and the 13762NF rat mammary adenocarcinoma in vivo. Anticancer Res. 2002;22(5):2685-92.

51. Hann HW, Stahlhut MW, Blumberg BS. Iron nutrition and tumor growth: decreased tumor growth in iron-deficient mice. Cancer Res. 1988;48(15):4168-70.

52. Sanvisens N, Bañó MC, Huang M, Puig S. Regulation of ribonucleotide reductase in response to iron deficiency. Mol Cell. 2011;44(5):759-69.

ARTICLE IN PRESS

ARTICLE IN PRESS

53. Xue X, Taylor M, Anderson E, Hao C, Qu A, Greenson JK, et al. Hypoxia-inducible factor-2alpha activation promotes colorectal cancer progression by dysregulating iron homeostasis. Cancer Res. 2012;72(9):2285-93.

54. Torti SV, Torti FM. Iron and cancer: more ore to be mined. Nat Rev Cancer. 2013;13(5):342-55.

55. Hann HW, Stahlhut MW, Menduke H. Iron enhances tumor growth. Observation on spontaneous mammary tumors in mice. Cancer. 1991;68(11):2407-10.

56. Wang F, Elliott RL, Head JF. Inhibitory effect of deferoxamine mesylate and low iron diet on the 13762NF rat mammary adenocarcinoma. Anticancer Res. 1999;19(1a):445-50.

57. Hrabinski D, Hertz JL, Tantillo C, Berger V, Sherman AR. Iron repletion attenuates the protective effects of iron deficiency in DMBA-induced mammary tumors in rats. Nutr Cancer. 1995;24(2):133-42.

58. Torti SV, Manz DH, Paul BT, Blanchette-Farra N, Torti FM. Iron and Cancer. Annu Rev Nutr. 2018;38:97-125.

59. Buss JL, Greene BT, Turner J, Torti FM, Torti SV. Iron chelators in cancer chemotherapy. Curr Top Med Chem. 2004;4(15):1623-35.

60. Shao J, Zhou B, Di Bilio AJ, Zhu L, Wang T, Qi C, et al. A Ferrous-Triapine complex mediates formation of reactive oxygen species that inactivate human ribonucleotide reductase. Mol Cancer Ther. 2006;5(3):586-92.

61. Blatt J, Stitely S. Antineuroblastoma activity of desferoxamine in human cell lines. Cancer Res. 1987;47(7):1749-50.

62. Greene BT, Thorburn J, Willingham MC, Thorburn A, Planalp RP, Brechbiel MW, et al. Activation of caspase pathways during iron chelator-mediated apoptosis. The Journal of biological chemistry. 2002;277(28):25568-75.

ARTICLE IN PRESS

ARTICLE IN PRESS

63. Simonart T, Degraef C, Andrei G, Mosselmans R, Hermans P, Van Vooren JP, et al. Iron chelators inhibit the growth and induce the apoptosis of Kaposi's sarcoma cells and of their putative endothelial precursors. J Invest Dermatol. 2000;115(5):893-900.

64. Richardson DR, Kalinowski DS, Lau S, Jansson PJ, Lovejoy DB. Cancer cell iron metabolism and the development of potent iron chelators as anti-tumour agents. Biochimica et Biophysica Acta (BBA) - General Subjects. 2009;1790(7):702-17.

65. Pfeifhofer-Obermair C, Tymoszuk P, Petzer V, Weiss G, Nairz M. Iron in the Tumor Microenvironment-Connecting the Dots. Front Oncol. 2018;8:549.

66. Abdelaal G, Veuger S. Reversing oncogenic transformation with iron chelation. Oncotarget. 2021;12(2):106-24.

67. Lui GY, Kovacevic Z, Richardson V, Merlot AM, Kalinowski DS, Richardson DR. Targeting cancer by binding iron: Dissecting cellular signaling pathways. Oncotarget. 2015;6(22):18748-79.

ARTICLE IN PRESS

Figure Legends

Figure 1. The study design and changes in HIF-1 signaling pathway in skin samples following DIDP-treatment. (A) Study design and timeline of the animal study. Experimental work was conducted using a murine xenograft human breast cancer model. Animals were randomly assigned to either the control or DFO group. Mice in the DFO group received daily DFO treatment via DIDP. Tumor growth was monitored weekly using a bioluminescence assay. Skin and tumor tissues were collected after 30 days of treatment. **(B)** Representative images (40x magnification) and **(C)** quantitative analysis of immunofluorescent staining of HIF-1 in control (Ctr) and DFO-treated (DFO) skin. In (B), yellow arrows indicate HIF-1-positive cells, dashed lines mark the epidermal-dermal junction, and nuclei are stained with DAPI (blue). **(D)** Relative expression of HIF-1 target genes (*Vegfa* and *Pdk1*) in control (Ctr)

ARTICLE IN PRESS

and DFO-treated (DFO) skin. **(E)** Representative images (10x magnification) and **(F)** quantitative analysis of immunofluorescent staining of CD31 in control (Ctr) and DFO-treated (DFO) skin. In (E), nuclei are stained with DAPI (blue). **(E')** shows a magnified view of the area marked by the dashed squares in panel E. In all graphs, data are presented as the average for all tested animals, and each dot represents the result for one animal. The average value for the controls was set as 1. Error bars represent SD. Statistical significance was calculated using the Mann-Whitney test: $**p \leq 0.01$, $****p \leq 0.0001$.

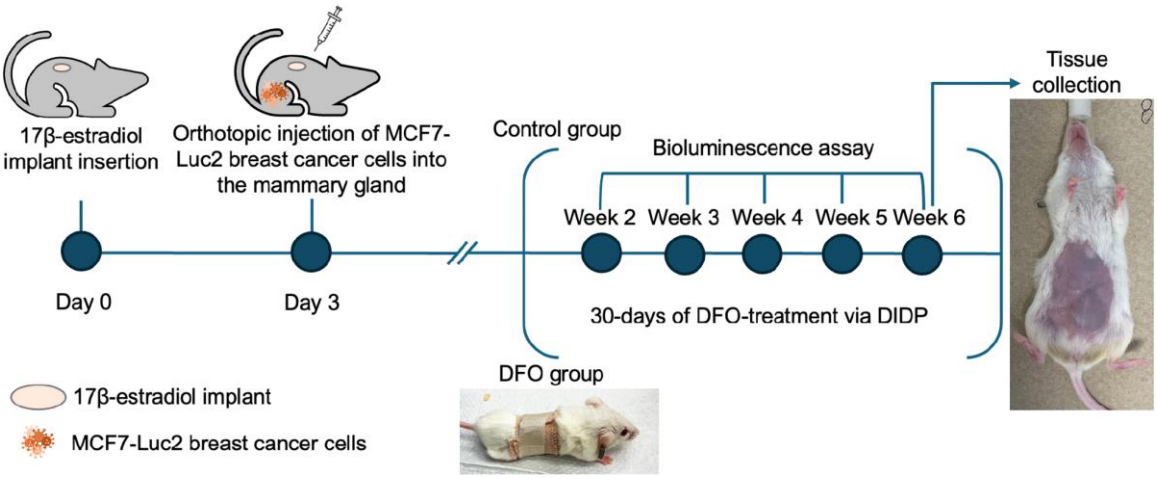
Figure 2. Effect of topical DFO treatment via DIDP on tumor growth. (A) Relative expression of HIF-1 target genes (*VEGFA* and *PDK1*) in tumor tissue excised from control (Ctr) and DFO-treated (DFO) mice. **(B)** Representative image and **(C)** quantitative analysis of weekly bioluminescence assays performed to monitor *in vivo* tumor growth in control (Ctr) and DFO-treated (DFO) mice. **(D)** Representative images, **(E)** weight, and **(F)** volume of tumors excised at the study endpoint from control (Ctr) and DFO-treated (DFO) mice. In all graphs, data are presented as the average for all tested animals, and in (A), (E), and (F), each dot represents the result for one animal. The average value for the controls was set as 1. In (A), (E), and (F), error bars represent SD, and in (C), error bars represent SEM. Statistical significance was calculated using the Mann-Whitney test.

ARTICLE IN PRESS

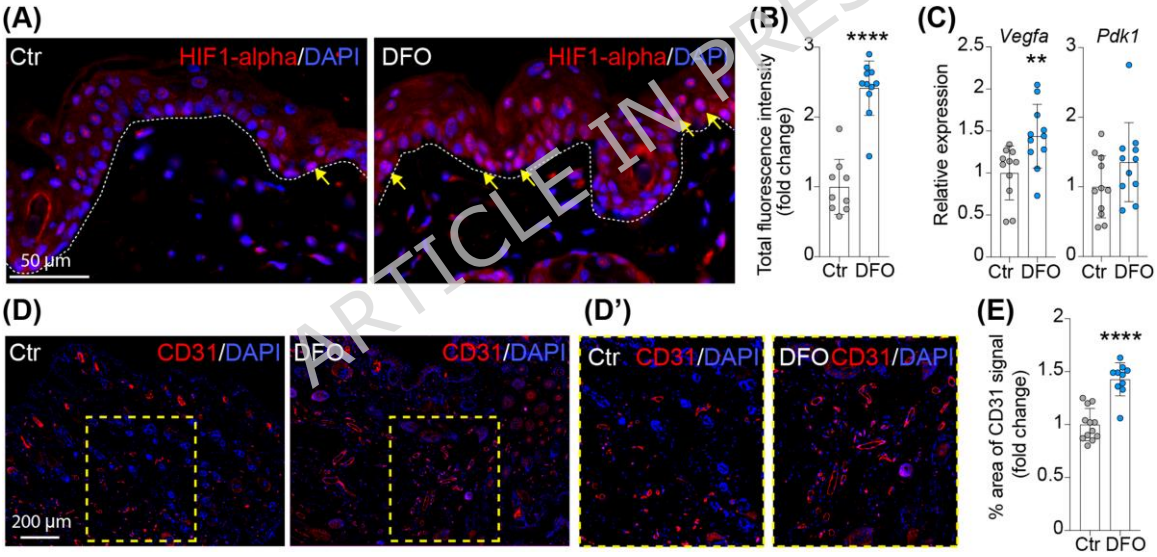
Figure 3. Effect of topical DFO treatment via DIDP on cancer cell proliferation and apoptosis. (A) Representative images (40x magnification) and **(B)** quantitative analysis of immunofluorescent staining of Ki-67 in tumor tissue excised from control (Ctr) and DFO-treated (DFO) mice. In (A), nuclei are stained with DAPI (blue). **(C)** Relative expression of *CCND1* in tumor tissue excised from control (Ctr) and DFO-treated (DFO) mice. (**D)** Representative images (25x magnification) and **(E)** quantitative analysis of TUNEL staining in tumor tissue excised from control (Ctr) and DFO-treated (DFO) mice. In (D), nuclei are stained with 7-AAD (blue). In all graphs, data are presented as the average for all tested

ARTICLE IN PRESS

animals, and each dot represents the result for one animal. The average value for the controls was set as 1. Error bars represent SD. Statistical significance was calculated using the Mann-



Whitney test: $*p \leq 0.05$.



ARTICLE IN PRESS

